Supplementary Information

N-methyl-β-carboline alkaloids: structure-dependent photosensitizing properties and localization in subcellular domains

M. Paula Denofrio, [a, †] *Federico A. O. Rasse-Suriani,* [a, b, †] *Jose M. Paredes,* [c] *Federico Fassetta,* [a] *Luis Crovetto* [c,*] *Maria D. Giron,* [d] *Rafael Salto,* [d] *Bernd Epe* [e] *and Franco M. Cabrerizo* [a,*]

[a] Instituto Tecnológico de Chascomús (INTECH), Universidad Nacional de San Martín (UNSAM) - Consejo Nacional de Investigaciones Científicas y Técnicas (CONICET), Av. Intendente Marino Km 8.2, CC 164 (B7130IWA), Chascomús, Argentina. E-mail: fcabrerizo@intech.gov.ar

[b] Instituto de Investigaciones Fisicoquímicas Teóricas y Aplicadas (INIFTA), CCT-La Plata, Universidad Nacional de La Plata, Diag. 113 y 64 (1900), La Plata, Argentina

[c] Department of Physical Chemistry, Faculty of Pharmacy, Unidad de Excelencia en Quimica Aplicada a Biomedicina y Medioambiente (UEQ), University of Granada, Cartuja Campus, 18071 Granada, Spain. E-mail: luiscrovetto@ugr.es

[d] Department of Biochemistry and Molecular Biology II, Faculty of Pharmacy, Unidad de Excelencia en Quimica Aplicada a Biomedicina y Medioambiente (UEQ), University of Granada, Cartuja Campus, 18071 Granada, Spain

[e] Institute of Pharmacy and Biochemistry, University of Mainz, Staudingerweg 5, Mainz, Germany.

* To whom correspondence should be addressed (fcabrerizo@intech.gov.ar and luiscrovetto@ugr.es)

† Equal contribution of both authors

Contents: **Page**

2. DNA damage profile photoinduced by 1a, 2a and 3a

(a)

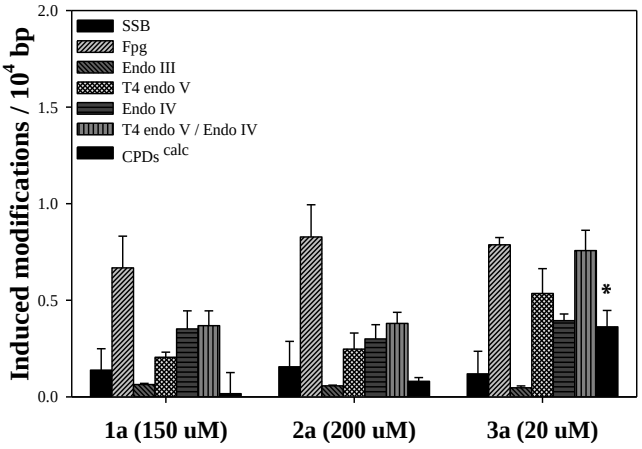

(b)

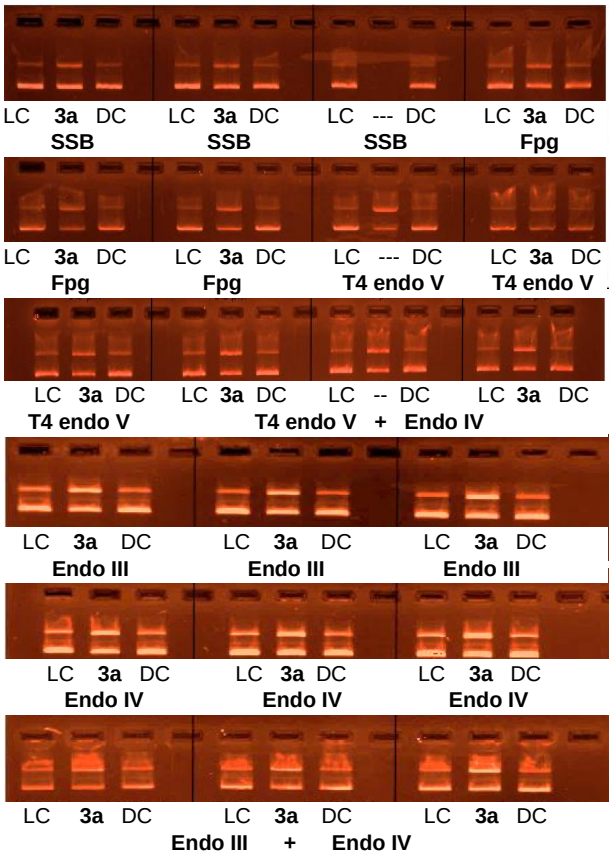

Figure SI.1. (a) DNA damage profiles showing the numbers of SSBs and several types of endonuclease sensitive modifications induced in PM2 DNA by photoexcited unsubstituted βCs (**1a**, **2a** and **3a,** concentrations are indicated in parenthesis). Data are taken from Ref. [38]. **(b)** Representative examples of electrophoretic runs of the experiments reported in the main text for **3b** (Figure 1a). LC (Light-control) means PM2 irradiated in the absence of **3a**), DC (Dark-control) means PM2 + **3a** (0.5 μM) in the absence of light) and **3a** means PM2 irradiated in the presence of **3a** (0.5 μM). Enzymes used in each case are depicted at the bottom of each gel.

2. Molar absorption coefficient of ctDNA: bibliographic data compilation

More than sixty years ago, Chargaff *et al.* (1953) [1] and Beaven *et al.* (1955) [2] reported values for molar absorption coefficient at 260 nm ($\varepsilon^{260\ nm}$) ranging from 6,000 to 9,000. A few years later, Felsenfeld *et al*. (1965) [3] and Hirschman *et al*. (1966) [4] reported for several DNA samples $\varepsilon^{260\ nm}$ average values ranging from 6,400 and 6,900 M^{-1} cm^{-1}. Changes in the local surroundings of the nucleobases in DNA subject to denaturing conditions (such as high temperature, extreme pHs and/or ionic strength) give rise to the major changes observed. DNA-composition, *i. e.*, ratio GC to AT base pairs, also plays a determining role in the average value of each DNA sample. However, in the particular case of calf thymus DNA (ctDNA) subject to nondenaturing physiological conditions (pH 7.4), $\varepsilon^{260\ nm}$ average values reported by Beaven *et al*. (1955), Chargaff *et al.* (1953) [1] and Hirschman *et al*. (1966) [4] differs by more than 35% (9,000 M^{-1} cm^{-1}, 6,650 (± 50) M^{-1} cm^{-1} and 6,280 (± 130) M^{-1} cm^{-1}, respectively).

The average $\varepsilon^{260\ nm}$ value mostly used among the scientific community to determine the nucleobase concentration in double-stranded DNA is of 6,500 - 6,700 M^{-1} cm^{-1} [5-21] or 13,100-13,200 Mbp^{-1} cm^{-1} (when is expressed in terms of base-pairs) [22-24]. A value of 7,000 M^{-1} cm^{-1} is also frequently used [25, 26]. Note that Fensenfeld's (1965) [3] and Hirschman's (1966) [4] manuscripts have been cited ~120 and ~80 times, respectively.[18] Although this quite low citation records, and according to one of the world's most popular internet search engines, more than 2,390,000 and 215,000 results matches with the search of "DNA + 6600" and "DNA + 13200", respectively.

However, the above-mentioned average value seems to be underestimated and, to date, is still somewhat controversial. As a first approximation, a direct average calculation based on the $\varepsilon^{260\ nm}$ values of the isolated deoxynucleotide dGMP, dAMP, dCMP and dTMP (12,180 M^{-1} cm^{-1}, 15,060 M^{-1} cm^{-1}, 7,100 M^{-1} cm^{-1} and 8,560 M^{-1} cm^{-1}, respectively)[27] normalized by the relative contribution of each base to the ctDNA sequence (*i.e.*, 42% and 58% of GC and AT base pairs, respectively)[4] leads to an average $\varepsilon^{260\ nm}$ value for ctDNA of 10,900 M^{-1} cm^{-1}. It has been well demonstrated that absorption coefficient decreases [28] when they are stacked in the double-stranded DNA helix. The extent of these changes also depends on the chemical structure of the neighboring nucleobase.[2] However, for all the nucleobases the relative decrease in the molar absorption coefficient of intact DNA is lower than 10%. Thus, the expected average $\varepsilon^{260\ nm}$ value of the nucleobase in ctDNA should be ~ 8,500 M^{-1} cm^{-1}. This hypothesis is supported by the fact that absorption coefficients reported for other type of DNA such as unpair deoxynucleotides oligomers (calculated with the nearest-neighbor approximation) ssDNA and/or dsDNA samples are considerably higher than that reported by Felsenfeld. *et al*. [29-31] In addition, in a recent study, Love *et al.* found that the general accepted average molar absorption coefficient of dsDNA would be underestimated. [32] Moreover, Love *et al.* suggest that the uncertainty in the molar absorption coefficient of dsDNA might be due to uncertainties in the original estimation of molar DNA content, based on the measurement of phosphorus content of their DNA samples.

3. References for “Molar absorption coefficient of ctDNA: bibliographic data compilation”:

1. E. Chargaff and R. Lipshitz, *Journal of the American Chemical Society*, 1953, **75**, 3658-3661.
2. G. H. Beaven, E. R. Holiday and E. A. Johnson, *In Chargaff, E. and Davidson, J.N. (eds), The Nucleic Acids. Academic Press, New York, NY, USA*, 1954, **1**, 493 - 553.
3. G. Felsenfeld and S. Z. Hirschman, *Journal of Molecular Biology*, 1965, **13**, 407-427.
4. S. Z. Hirschman and G. Felsenfeld, *Journal of Molecular Biology*, 1966, **16**, 347-358.
5. F. Ahmadi, N. Jamali, R. Moradian and B. Astinchap, *DNA and Cell Biology*, 2012, **31**, 259-268.
6. M. M. Gonzalez, M. Pellon-Maison, M. A. Ales-Gandolfo, M. R. Gonzalez-Baró, R. Erra-Balsells and F. M. Cabrerizo, *Org. Biomol. Chem.*, 2010, **8**, 2543-2552.
7. H. Arthanari, S. Basu, T. L. Kawano and P. H. Bolton, *Nucleic Acids Research*, 1998, **26**, 3724-3728.
8. S. Z. Bathaie, A. A. Moosavi-Movahedi and A. A. Saboury, *Nucleic Acids Research*, 1999, **27**, 1001-1005.
9. S. T. Sigurdsson and F. Eckstein, *Nucleic Acids Research*, 1996, **24**, 3129-3133.
10. R. G. Eason, D. M. Burkhardt, S. J. Phillips, D. P. Smith and S. S. David, *Nucleic Acids Research*, 1996, **24**, 890-897.
11. A. K. Eggleston, N. A. Rahim and S. C. Kowalczykowski, *Nucleic Acids Research*, 1996, **24**, 1179-1186.
12. H. J. Karlsson, M. Eriksson, E. Perzon, B. Åkerman, P. Lincoln and G. Westman, *Nucleic Acids Research*, 2003, **31**, 6227-6234.
13. I. V. Kutyavin, D. Milesi, Y. Belousov, M. Podyminogin, A. Vorobiev, V. Gorn, E. A. Lukhtanov, N. M. J. Vermeulen and W. Mahoney, *Nucleic Acids Research*, 2006, **34**, e128-e128.
14. W. Wang, G. J. Lee, K. J. Jang, T. S. Cho and S. K. Kim, *Nucleic Acids Research*, 2008, **36**, e85-e85.
15. R. Marty, C. N. N'Soukpoé-Kossi, D. Charbonneau, C. M. Weinert, L. Kreplak and H.-A. Tajmir-Riahi, *Nucleic Acids Research*, 2009, **37**, 849-857.
16. D. Ghoshdastidar and S. Senapati, *Nucleic Acids Research*, 2018, **46**, 4344-4353.
17. P. Friedhoff, B. Kolmes, O. Gimadutdinow, W. Wende, K. L. Krause and A. Pingoud, *Nucleic Acids Research*, 1996, **24**, 2632-2639.
18. B. Åkerman and E. Tuite, *Nucleic Acids Research*, 1996, **24**, 1080-1090.
19. N. Korolev, N. V. Berezhnoy, K. D. Eom, J. P. Tam and L. Nordenskiöld, *Nucleic Acids Research*, 2009, **37**, 7137-7150.
20. L. H. Fornander, K. Frykholm, A. Reymer, A. Renodon-Cornière, M. Takahashi and B. Nordén, *Nucleic Acids Research*, 2012, **40**, 4904-4913.
21. A. Prisecaru, Z. Molphy, R. G. Kipping, E. J. Peterson, Y. Qu, A. Kellett and N. P. Farrell, *Nucleic Acids Research*, 2014, **42**, 13474-13487.
22. V. R. Machha, J. R. Waddle, A. L. Turner, S. Wellman, V. H. Le and E. A. Lewis, *Biophysical Chemistry*, 2013, **184**, 22-28.
23. M. M. Gonzalez, M. Vignoni, M. Pellon-Maison, M. A. Ales-Gandolfo, M. R. Gonzalez-Baro, R. Erra-Balsells, B. Epe and F. M. Cabrerizo, *Org. Biomol. Chem.*, 2012, **10**, 1807-1819.
24. X. Li, Y. Peng and X. Qu, *Nucleic Acids Research*, 2006, **34**, 3670-3676.
25. S. D. Kennedy and R. G. Bryant, *Biophysical Journal*, 1986, **50**, 669-676.
26. S. Kashanian, M. B. Gholivand, F. Ahmadi, A. Taravati and A. H. Colagar, *Spectrochim Acta A Mol Biomol Spectrosc*, 2007, **67**, 472-478.
27. M. J. Cavaluzzi and P. N. Borer, *Nucleic Acids Research*, 2004, **32**, e13-e13.
28. S. Zamenhof and E. Chargaff, *Journal of Biological Chemistry*, 1949, **178**, 531-532.
29. C.-C. Chang, C.-W. Chien, Y.-H. Lin, C.-C. Kang and T.-C. Chang, *Nucleic Acids Research*, 2007, **35**, 2846-2860.
30. N. Sugimoto, R. Kierzek, S. M. Freier and D. H. Turner, *Biochemistry*, 1986, **25**, 5755-5759.
31. D. M. Gray, S.-H. Hung and K. H. Johnson, in *Methods Enzymol.*, Academic Press, 1995, vol. 246, pp. 19-34.
32. J. L. Love, P. Scholes, B. Gilpin, M. Savill, S. Lin and L. Samuel, *Journal of Microbiological Methods*, 2006, **67**, 349-356.

4. Microwave Plasma-Emission Atomic Spectroscopy (MP-EAS) analysis

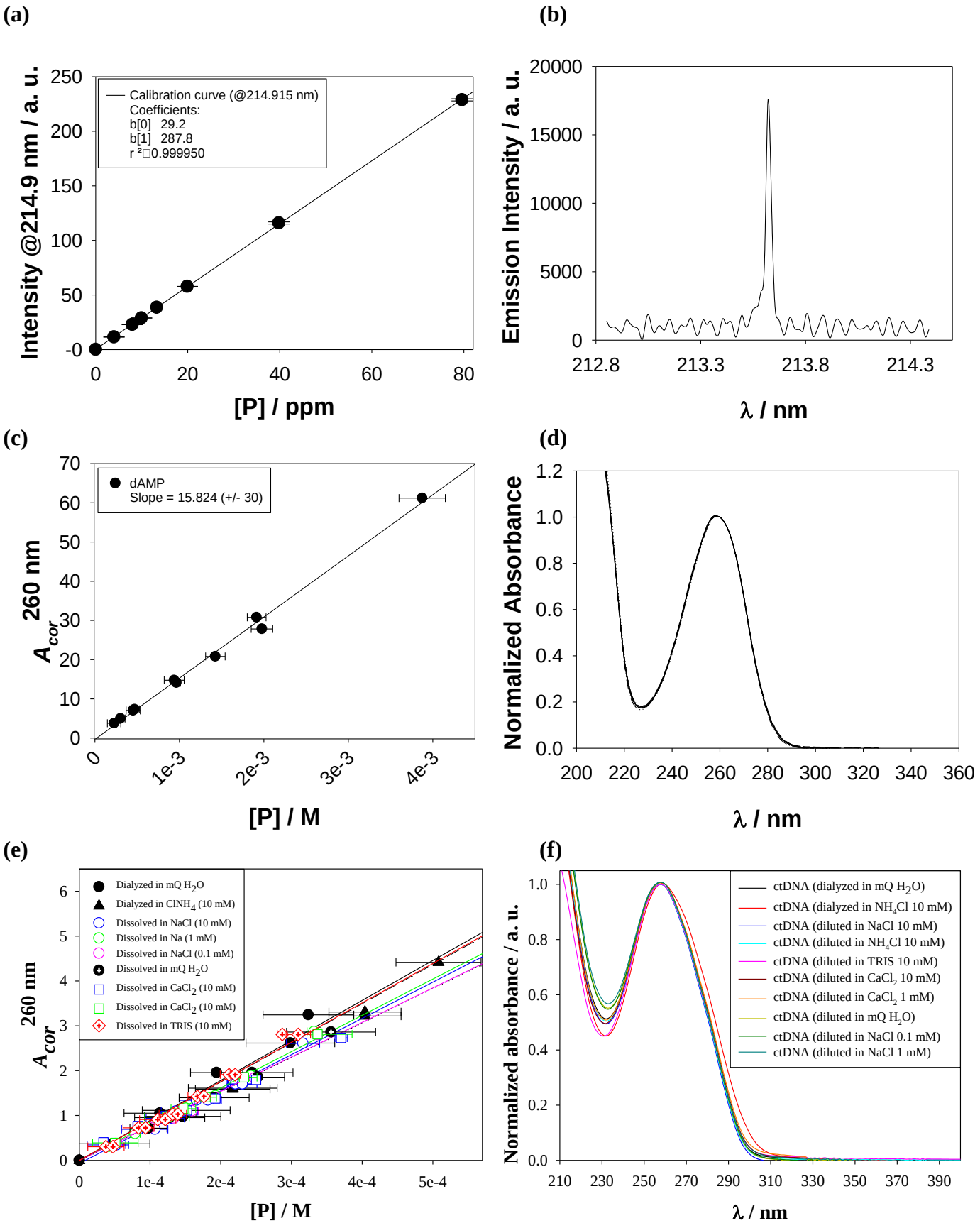

Figure SI.2. (a) Calibration curves for phosphate quantification. **(b)** Representative MP-EAS signal of phosphate emission. **(c)** Absorbance of dAMP aqueous solution at 260 nm ($A^{260\ nm}$) vs phosphate concentration ([P]). **(d)** UV-visible normalized absorption spectra of the corresponding dAMP aqueous solutions depicted in figure (c). **(e)** Absorbance of different ctDNA solutions at 260 nm ($A^{260\ nm}$) vs phosphate concentration ([P]). Data obtained from three independent experiments. **(f)** Representative normalized absorption spectra of the different ctDNA solutions.

5. Interaction between 1b and ctDNA: steady-state fluorescence study vs pH.

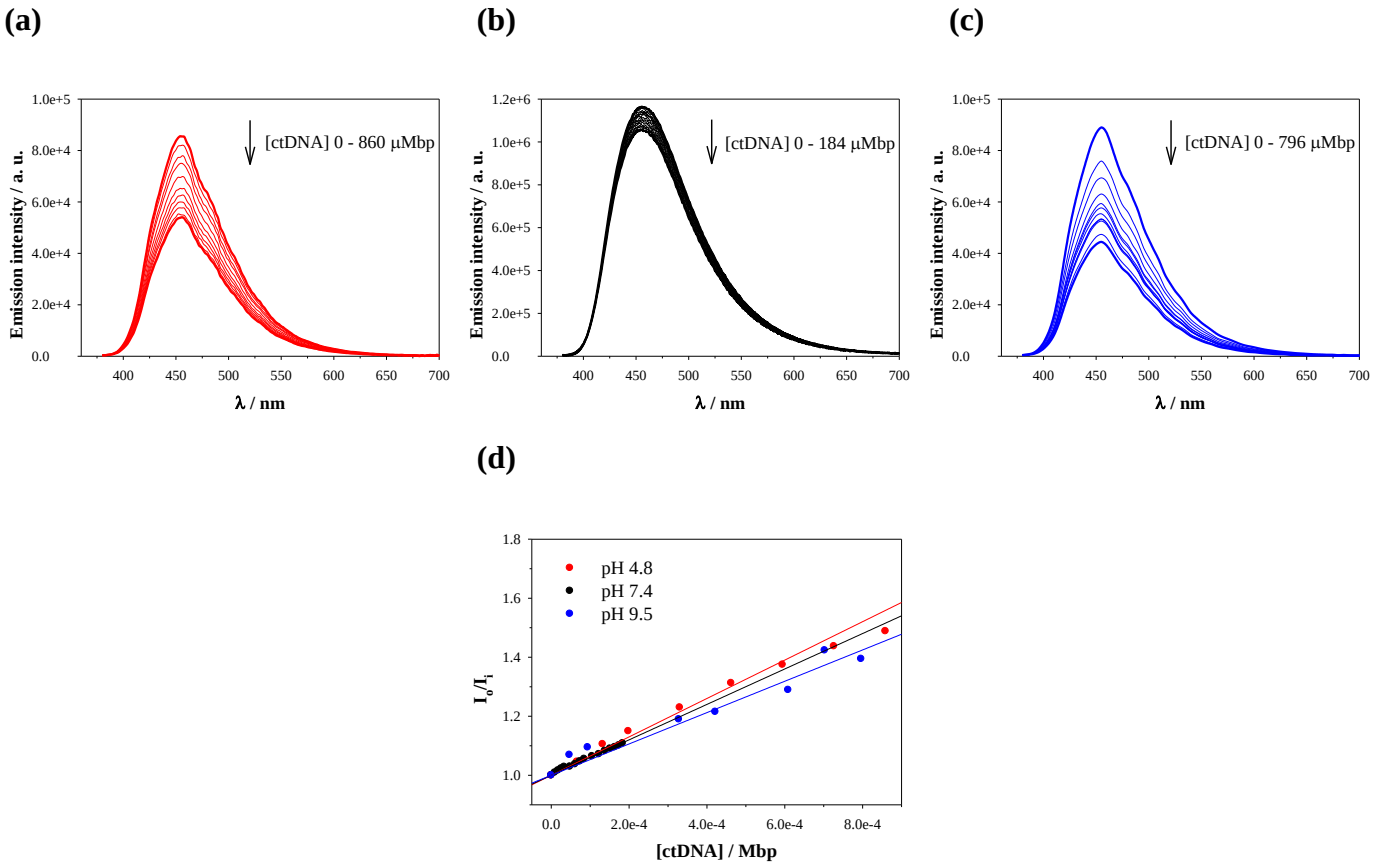

Figure SI.3. Corrected fluorescence emission spectra of **1b** (30 μM, λ_{exc} = 374 nm) buffered solution recorded in the presence of increasing amounts of ctDNA at pH: **(a) 4.8 (acetate buffer)**, **(b) 7.4 (phosphate buffer)** and **(c) 9.5 (borax buffer)**. Arrows indicate the variation in the emission spectra upon increasing [ctDNA] (μMbp, initial and final concentrations are highlighted). **(d)** Stern–Volmer plots of the total fluorescence emission calculated as the integral below the whole emission bands of spectra depicted in (a), (b) and (c).

6. Interaction between 1c and ctDNA: steady-state fluorescence study vs pH.

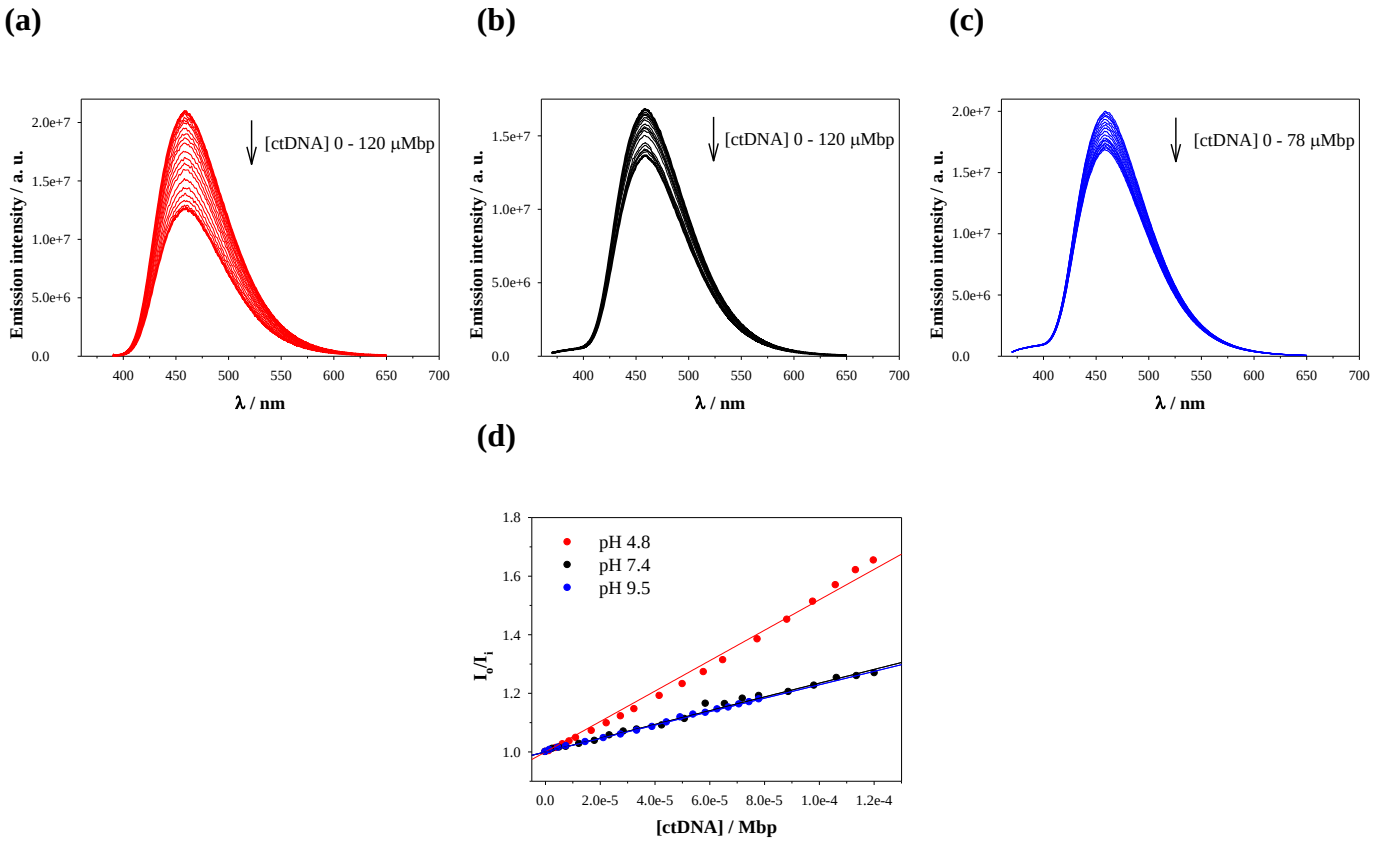

Figure SI.4. Corrected fluorescence emission spectra of **1c** (20 μM) buffered solution recorded in the presence of increasing amounts of ctDNA at pH: **(a) 4.8 (acetate buffer, λ_{exc} = 374 nm)**, **(b) 7.4 (phosphate buffer, λ_{exc} = 365 nm)** and **(c) 9.5 (borax buffer, λ_{exc} = 362 nm)**. Arrows indicate the variation in the emission spectra upon increasing [ctDNA] (μMbp, initial and final concentrations are highlighted). **(d)** Stern–Volmer plots of the total fluorescence emission calculated as the integral below the whole emission bands of spectra depicted in (a), (b) and (c).

7. Interaction between 1d and ctDNA: steady-state fluorescence study vs pH.

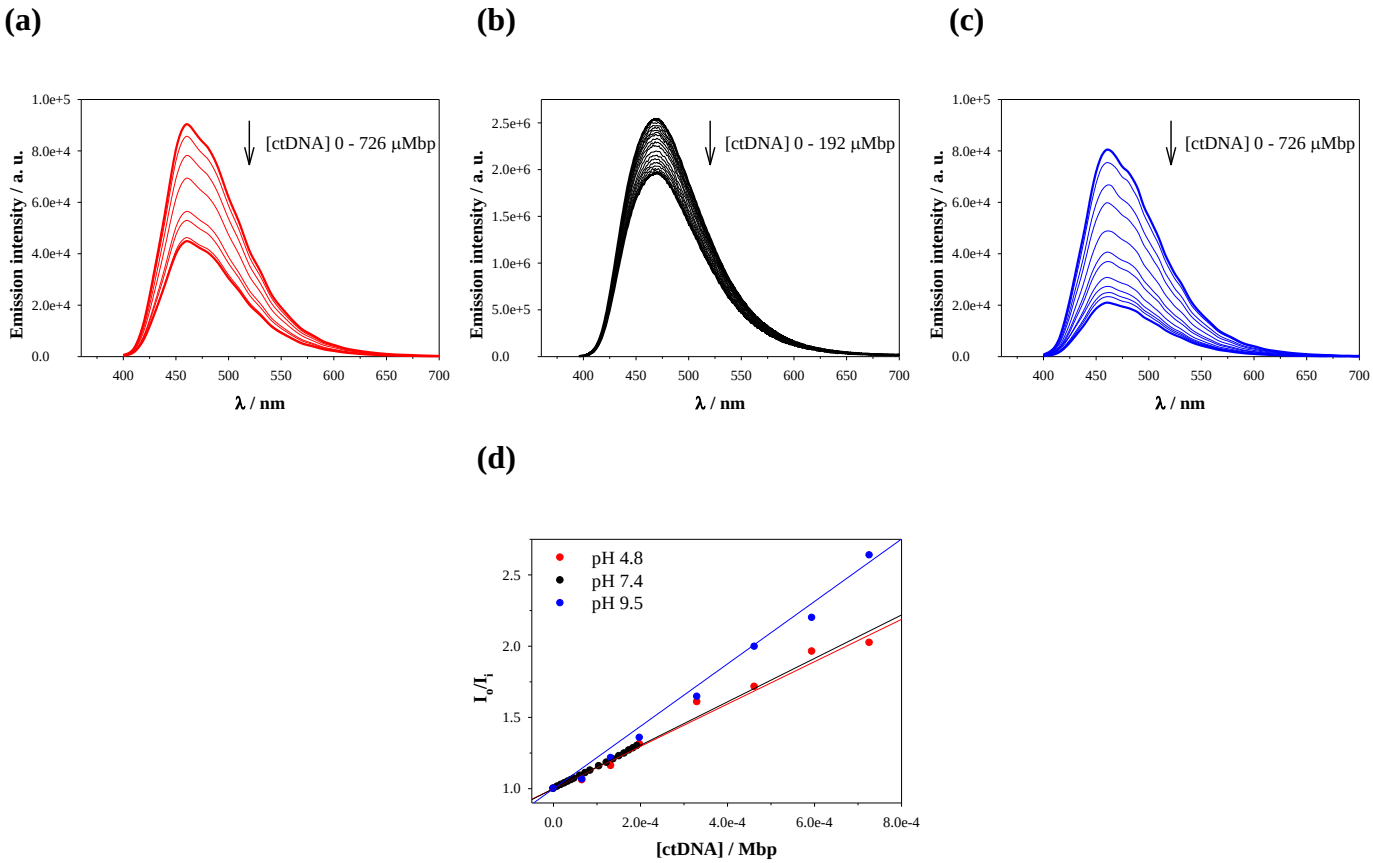

Figure SI.5. Corrected fluorescence emission spectra of **1d** (30 μM, λ_{exc} = 388 nm) buffered solution recorded in the presence of increasing amounts of ctDNA at pH: **(a) 4.8 (acetate buffer)**, **(b) 7.4 (phosphate buffer)** and **(c) 9.5 (borax buffer)**. Arrows indicate the variation in the emission spectra upon increasing [ctDNA] (μMbp, initial and final concentrations are highlighted). **(d)** Stern–Volmer plots of the total fluorescence emission calculated as the integral below the whole emission bands of spectra depicted in (a), (b) and (c).

8. Interaction between 2c and ctDNA: steady-state fluorescence study vs pH.

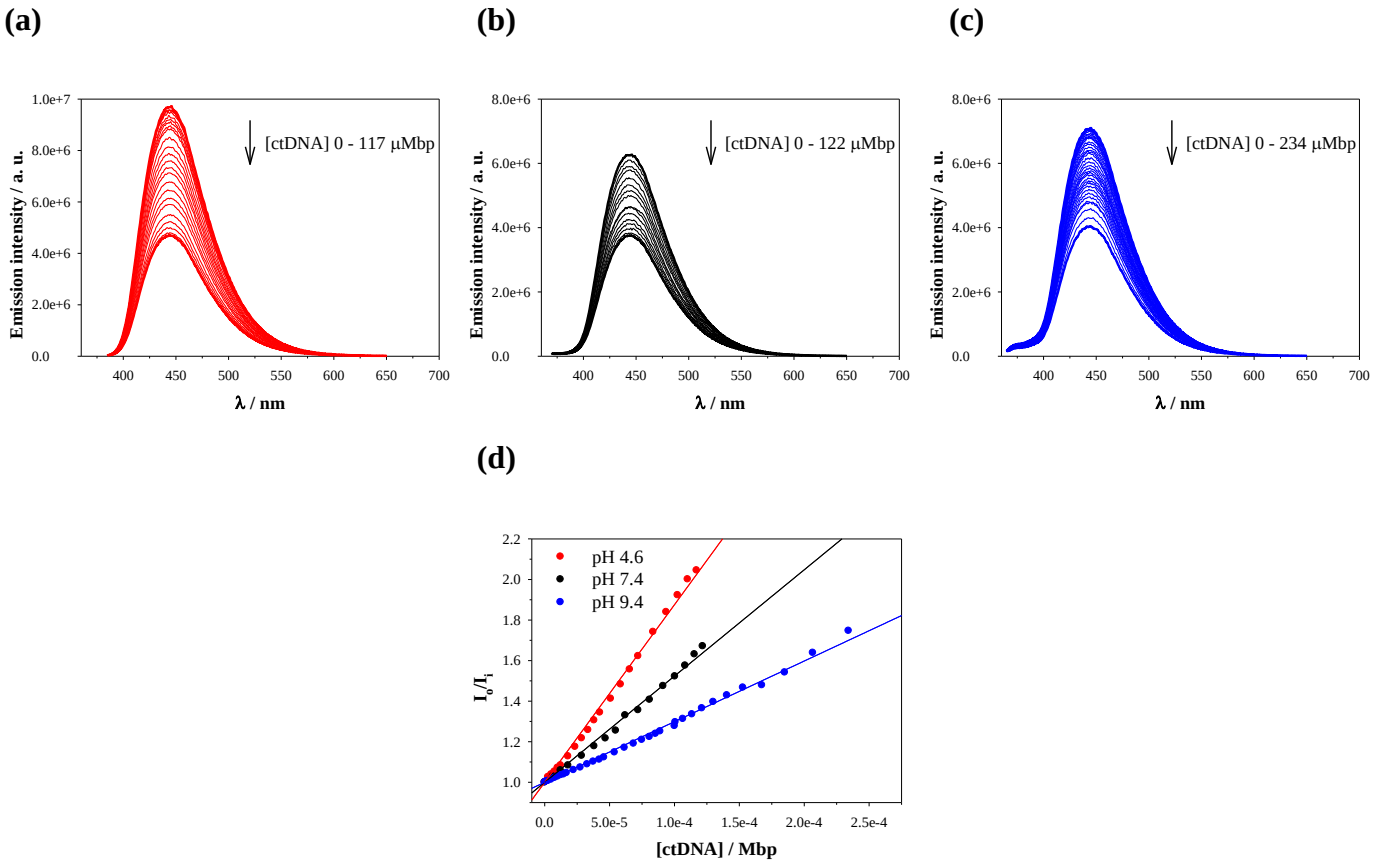

Figure SI.6. Corrected fluorescence emission spectra of **2c** (20 μM) buffered solution recorded in the presence of increasing amounts of ctDNA at pH: **(a) 4.8 (acetate buffer, λ_{exc} = 377 nm)**, **(b) 7.4 (phosphate buffer, λ_{exc} = 365 nm)** and **(c) 9.5 (borax buffer, λ_{exc} = 360 nm)**. Arrows indicate the variation in the emission spectra upon increasing [ctDNA] (μMbp, initial and final concentrations are highlighted). **(d)** Stern–Volmer plots of the total fluorescence emission calculated as the integral below the whole emission bands of spectra depicted in (a), (b) and (c).

9. Interaction between 3c and ctDNA: steady-state fluorescence study vs pH.

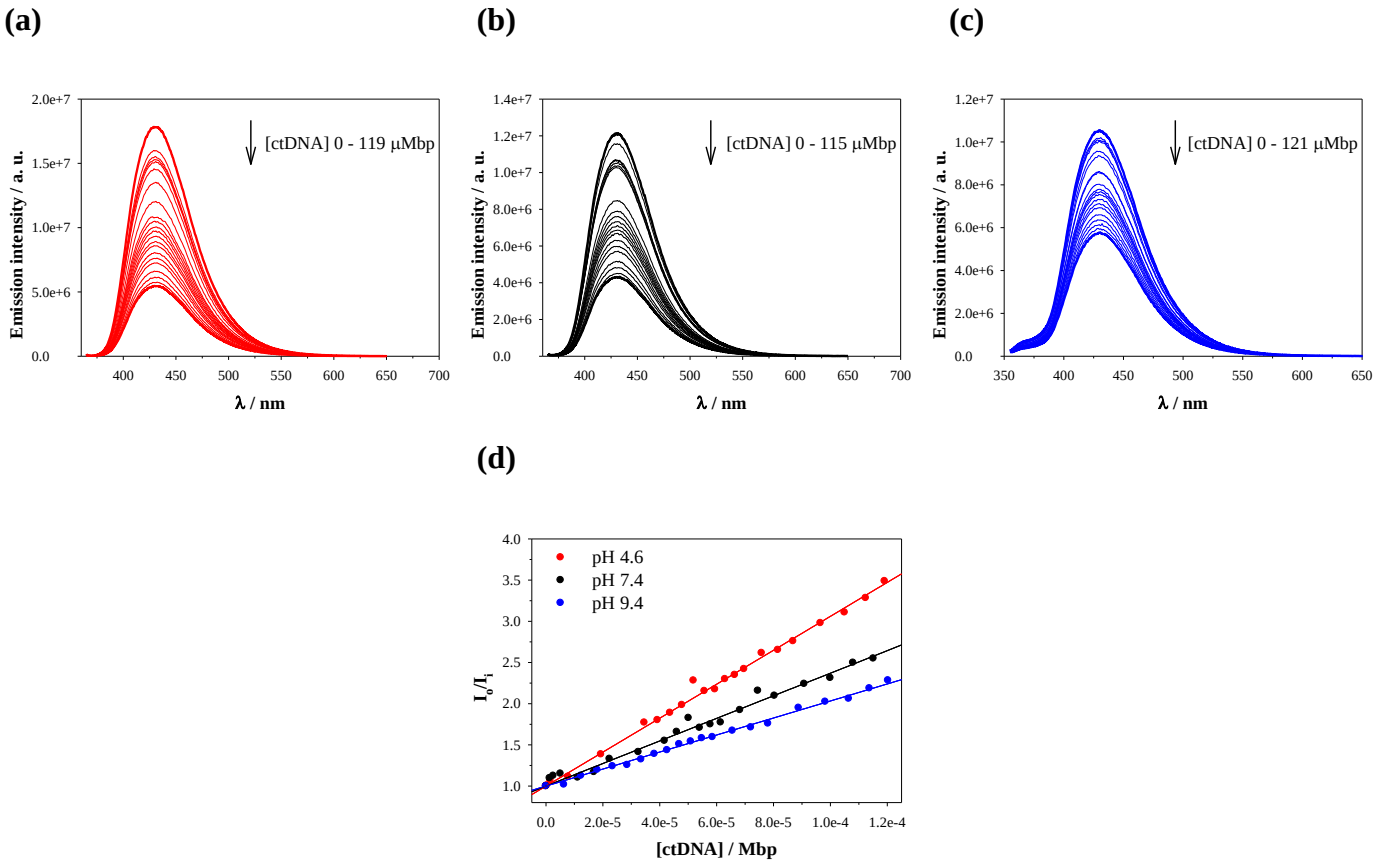

Figure SI.7. Corrected fluorescence emission spectra of **3c** (15 μM) buffered solution recorded in the presence of increasing amounts of ctDNA at pH: **(a) 4.8 (acetate buffer, λ_{exc} = 360 nm)**, **(b) 7.4 (phosphate buffer, λ_{exc} = 360 nm)** and **(c) 9.5 (borax buffer, λ_{exc} = 350 nm)**. Arrows indicate the variation in the emission spectra upon increasing [ctDNA] (μMbp, initial and final concentrations are highlighted). **(d)** Stern–Volmer plots of the total fluorescence emission calculated as the integral below the whole emission bands of spectra depicted in (a), (b) and (c).

10 Interaction between 1b and 2b with ctDNA: Stern-Volmer plot (pH 7.4)

(a)

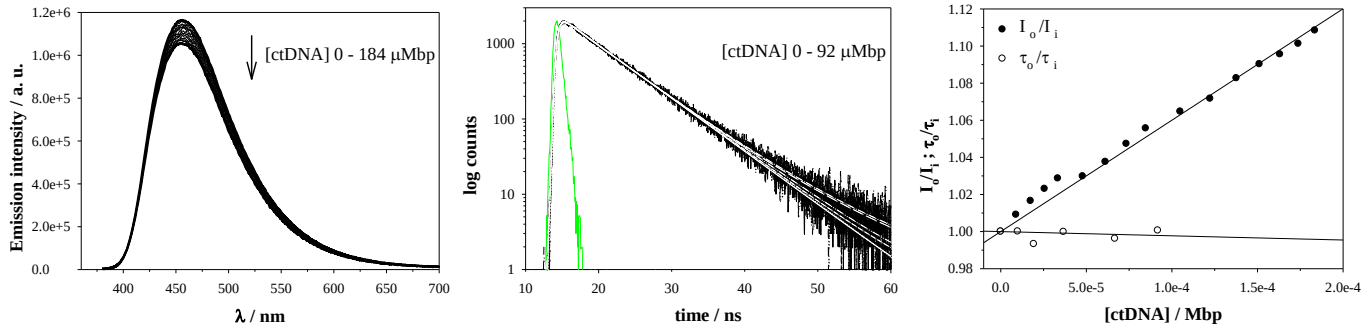

(b)

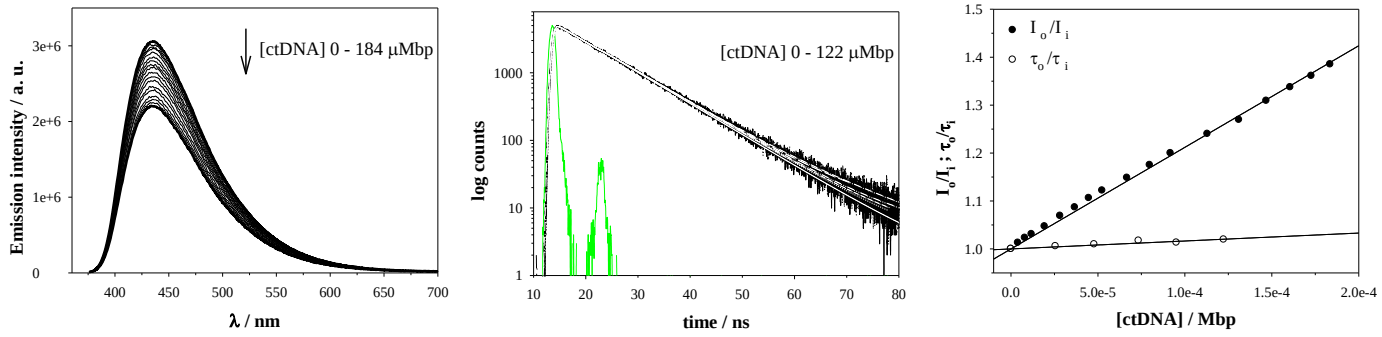

Figure SI.8. *Left column:* Corrected fluorescence emission spectra of: **(a) 1b** (35 μM, λ_{exc} = 374 nm) and **(b) 2b** (30 μM, λ_{exc} = 368 nm) buffered solution (pH 7.4) recorded in the presence of increasing amounts of ctDNA. Arrows indicate the variation in the [ctDNA] (μMbp). *Middle column*: the corresponding fluorescence decays recorded in air-equilibrated solutions (λ_{exc} = 341 nm and λ_{em} = 454 nm), prompt signal (green line) and mono-exponential fitting curves (white lines). *Right column*: Stern–Volmer plots of the fluorescence intensities (I_F, calculated as the integral below the whole emission spectra) and lifetimes (τ_F).

11 Interaction between 1d and 2d with ctDNA: Stern-Volmer plot (pH 7.4)

(a)

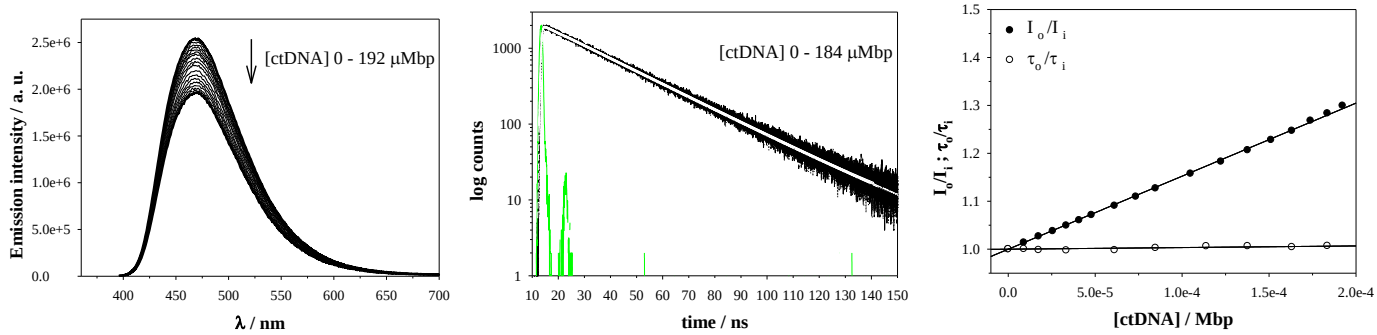

(b)

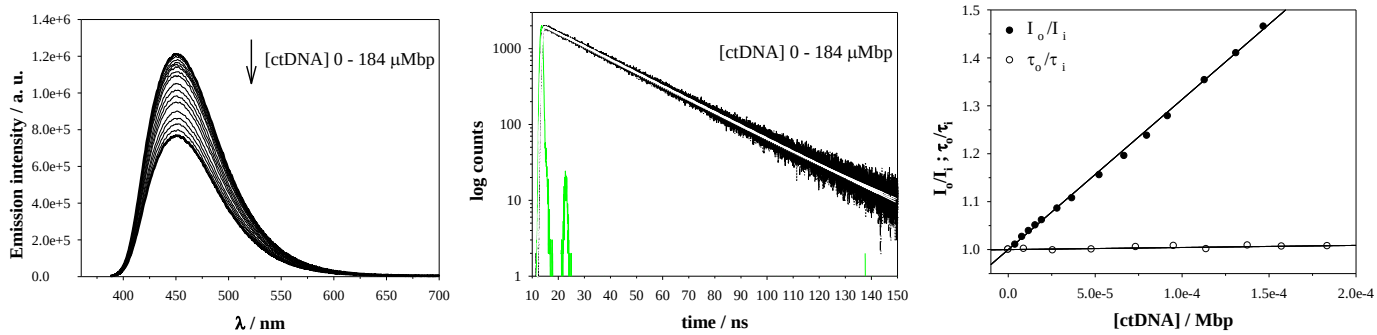

Figure SI.9. *Left column:* Corrected fluorescence emission spectra of: **(a) 1d** (35 µM, λ_{exc} = 388 nm) and **(b) 2d** (25 µM, λ_{exc} = 380 nm) buffered solution (pH 7.4) recorded in the presence of increasing amounts of ctDNA. Arrows indicate the variation in the [ctDNA] (Mbp). *Middle column*: the corresponding fluorescence decays recorded in air-equilibrated solutions (λ_{exc} = 341 nm and λ_{em} = 454 nm), prompt signal (green line) and mono-exponential fitting curves (white lines). *Right column*: Stern–Volmer plots of the fluorescence intensities (I_F, calculated as the integral below the whole emission spectra) and lifetimes (τ_F).

12 Fluorescence images from HEK239 cell co-incubated with βCs obtained before and after washing with PBS

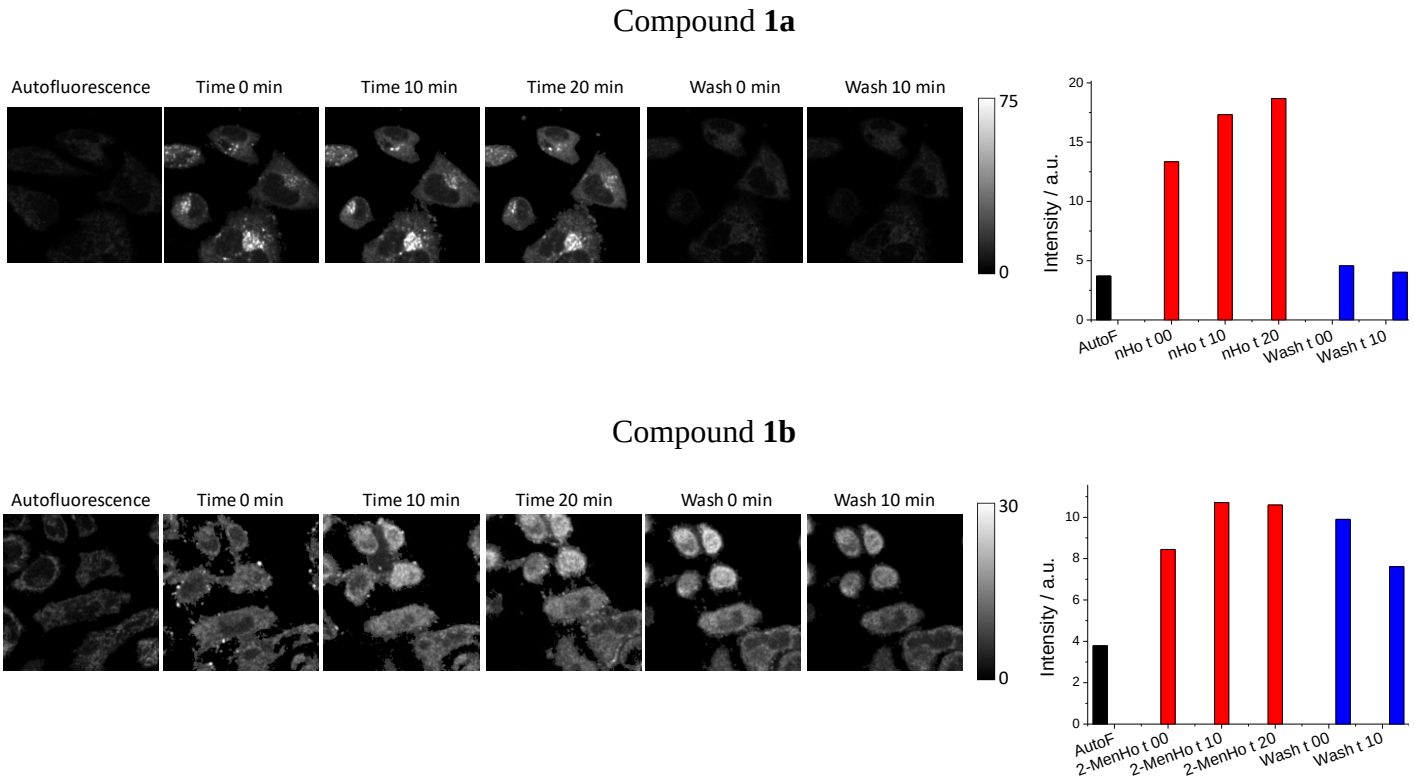

Figure SI.10. Examples of fluorescence images obtained from HEK293 cells co-incubated with **1a** and **1b.** Column 1 represents the HEK293 autofluorescence. Columns 2 to 4 represent fluorescence images obtained after 0, 10 and 20 minutes of addition of the corresponding βC, respectively. Columns 5 and 6, show images obtained 0 and 10 minutes after washing HEK293 cells with PBS. Bar plot on the right shows the average fluorescence intensity of cells depicted on the left side.

13 Pearson coefficient calculations

The Pearson coefficient (r) was calculated following the next equation:

$$r = \frac{\sum(x - \bar{x})(y - \bar{y})}{\sqrt{\sum(x - \bar{x})^2 \sum(y - \bar{y})^2}}$$

x and *y* are the pixel values and $\bar{x}$ and $\bar{y}$ are the mean of all the pixel matrix. We calculated *r* using a home-made macro in *Fiji is just imagej* (see brelow) where the matrix $(x - \bar{x})$, $(y - \bar{y})$, $(x - \bar{x})^2$ and $(y - \bar{y})^2$ where calculated. Later, the math operations requested to obtain the Pearson coefficient.

```
//The macro calculates the Pearson coefficient of two images, named "C1" and "C2"
	selectWindow("C1")
	run("Duplicate...", "title=C1-ROI duplicate");
//It is necessary to select manually the threshold for both images
	runMacro("waitForUser-binary");
	run("Divide...", "value=255 stack");
	selectWindow("C2")
	run("Duplicate...", "title=C2-ROI duplicate");
	runMacro("waitForUser-binary");
	run("Divide...", "value=255 stack");
	selectWindow("C1")
	run("Duplicate...", "title=C1-Mean duplicate");
	runMacro("measure stack");
	frames=nSlices;
	run("Set Measurements...", " mean redirect=None decimal=4");
	for(i=0; i<frames; i++) {
	run("Clear Results");
	currentslice=i+1;
	setSlice(currentslice);
	run("Measure");
	run("Subtract...", "value="+getResult("Mean", 0));
	run("Clear Results");
	}
	selectWindow("C2");
	run("Duplicate...", "title=C2-Mean duplicate");
	runMacro("measure stack");
	frames=nSlices;
	run("Set Measurements...", " mean redirect=None decimal=4");
	for(i=0; i<frames; i++) {
	run("Clear Results");
	currentslice=i+1;
	setSlice(currentslice);
	run("Measure");
	run("Subtract...", "value="+getResult("Mean", 0));
	run("Clear Results");
	}
	imageCalculator("Multiply stack", "C1-Mean", "C1-ROI");
	imageCalculator("Multiply stack", "C2-Mean", "C2-ROI");
	imageCalculator("Multiply create 32-bit stack", "C1-Mean","C2-Mean");
	rename ("C1-Mean*C2-Mean");
	selectWindow("C1-Mean");
	run("Duplicate...", "title=C1-Mean-sq duplicate");
	run("Square", "stack");
	run("Clear Results");
	run("Set Measurements...", "mean integrated redirect=None decimal=4");
	selectWindow("C2-Mean");
	run("Duplicate...", "title=C2-Mean-sq duplicate");
	run("Square", "stack");
	run("Clear Results");
	run("Set Measurements...", "mean integrated redirect=None decimal=4");
	selectWindow("C1-Mean-sq");
	run("Measure");
	selectWindow("C2-Mean-sq");
	run("Measure");
	den1=getResult("RawIntDen", 0);
	den2=getResult("RawIntDen", 1);
	Den0=(den1*den2);
	Den=(sqrt(Den0));
	run("Clear Results");
	selectWindow("C1-Mean*C2-Mean");
	run("Measure");
	Num    =getResult("RawIntDen", 0);
	R = Num/Den;
	print("\\Clear");
	print("R="+R);
	}
```

14 Fluorescence images from HeLa cell co-incubated with compound 1d and Mitotracker®

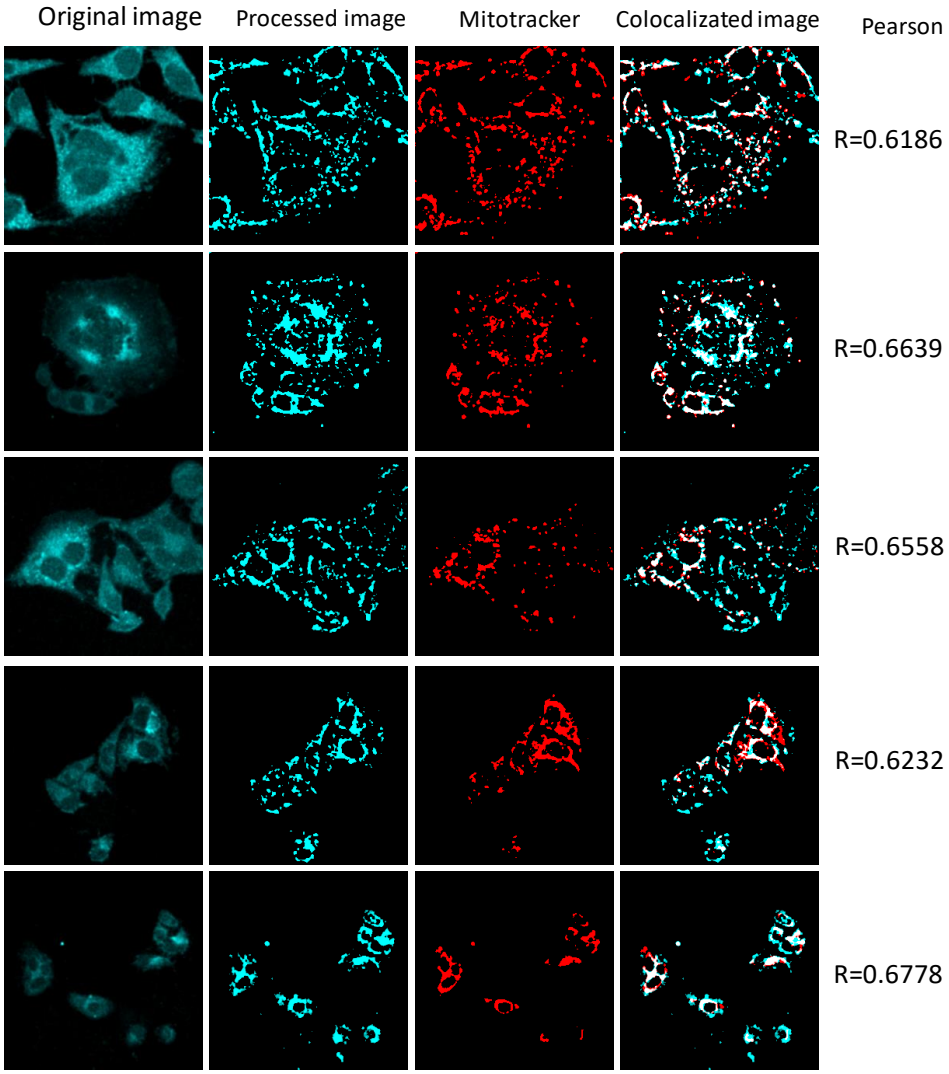

Figure SI.11. Fluorescence images of HeLa cells co-incubated with compound **1d** (cyan). The figure shows the raw fluorescence images (*first column*) and the processed images isolating the regions where the compound accumulates. Biomarker (red) Mitotracker® is in the *third column*. The merge from processed and biomarker images and the colocalization pixels (white) are represented in the *fourth column*.

15 Fluorescence images from HeLa cell co-incubated with compound 1d and Lysotracker®

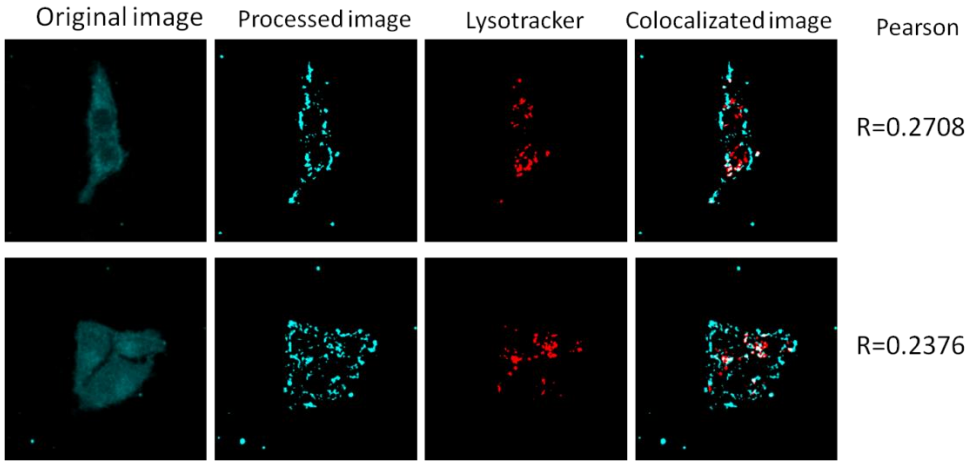

Figure SI.12. Fluorescence images of HeLa cells co-incubated with compound **1d** (cyan). The figure shows the raw fluorescence images (*first column*) and the processed images isolating the regions where the compound accumulates. Biomarker (red) Lysotracker® is in the *third column*. The merge from processed and biomarker images and the colocalization pixels (white) are represented in the *fourth column*.